Subcritical Bifurcations and Nonlinear Balloons in Faraday Waves

Peilong Chen and Kuo-An Wu
Department of Physics and Center for Complex Systems, National Central University, Chungli 320, Taiwan
(Received 2 May 2000)

Bicritical points at wave numbers k_b larger than the critical wave numbers k_c are found in parametric surface waves (Faraday waves) using both numerical simulations and nonlinear analysis. Because k_b-k_c is small, it is argued that subcritical bifurcations at $k > k_b$ can be easily observed in experiments. In the second part we present a generic argument predicting the existence of nonlinear states resembling a balloon outside the instability region. The prediction is confirmed in simulations and it is argued to apply to other systems with similar instability curves.

PACS numbers: 47.20.Ky, 47.35.+i, 47.54.+r

Parametric surface waves have been recently studied as a pattern formation in dissipative systems [1]. They are fluid surface waves, also called Faraday waves, that are generated by a vertical vibration [2]. The linear instability in an ideal fluid was studied [3]. The complete linear analysis of a viscous fluid, however, has been worked out only recently [4], although the driving threshold can be computed only numerically. Subsequently, analytical expansions of thresholds at small dampings were derived [5,6].

Extended regular patterns have been observed in experiments [7] near the threshold, and particularly interesting are the observations of the quasiperiodic patterns with fivefold, eightfold, and tenfold symmetries. In earlier theoretical attempts [8,9], standing wave amplitude equations were derived in the context of an ideal fluid flow, plus a damping postulate, to explain the patterns. However, these calculations cannot explain the variety of patterns observed. Rigorous derivation was later given [6], and its prediction agrees very well quantitatively with the observations. Recently, more patterns have been obtained in experiments using non-Newtonian fluids [10].

Hysteresis of the Faraday wave instability has also been observed when the wave was driven out of the resonance frequency [11,12], indicating a subcritical bifurcation. Amplitude equations up to the fifth order were derived to predict the hysteresis boundary [8,12–14]. However, these calculations were again based on the Lagrangian method [15], which neglects the rotational component of the flow. As indicated in [6], the lowest order contributions to the cubic damping coefficient are of the same order for both irrotational and rotational components of the flow. Hence the latter cannot be neglected in a nonlinear theory, even in the limit of small dissipations.

In this paper we first study bifurcation behaviors at different wave numbers by using rigorous nonlinear analysis [6] and numerical simulations of the incompressible Navier-Stokes equations. Near the critical driving, it is equivalent to tune the wave number or driving frequency. Bicritical points are found separating the supercritical and subcritical bifurcations. Their locations are obtained and the hysteresis boundaries can be determined in simulations. In the second part, we discuss waves near the tip of the neutral stability boundary. A generic argument shows an interesting formation of nonlinear states resembling a balloon in the wave amplitude-driving strength space. This prediction is confirmed by the simulations.

Two-dimensional numerical simulations are done for incompressible fluids with free upper surfaces and rigid flat bottoms. Periodic boundary conditions are used in the horizontal direction. A dynamical boundary conforming grid system changing with the free surface is generated by the Poisson equations,

$$\nabla^2 \xi(x,z) = P(x,z), \qquad \nabla^2 \zeta(x,z) = Q(x,z).$$

Here (x,z) is the physical coordinate and (ξ,ζ) is the Cartesian coordinate in a square computational domain. The functions P and Q control mapping between (x,z) and (ξ,ζ) [16].

Time evolution of the flow field $\mathbf{v}$ is computed with a semi-implicit time marching scheme of incompressible Navier-Stokes equations in the comoving frame (moving with the vertical vibration),

$$\frac{\partial \mathbf{v}}{\partial t} + (\mathbf{v}\cdot\nabla)\mathbf{v} = -\frac{1}{\rho}\nabla p + \frac{\nu}{\rho}\nabla^2\mathbf{v} - G(t)\hat{\mathbf{z}}. \quad (1)$$

Here ρ is the fluid density, ν the viscosity, and $G(t) = g_r + f\cos\omega t$, with g_r the gravitational acceleration, f the driving amplitude, and ω the driving frequency. Because there is no evolution equation for the pressure p, we take $\nabla\cdot$ of Eq. (1) to obtain a pressure Poisson equation with only spatial derivatives [17]. On the free surface, pressure is determined by the normal stress condition involving surface tension σ. The surface velocity, which gives the evolution of the free surface, is determined by the tangential stress condition. On the flat bottom standard no-slip conditions are used. Finally, the Poisson equations are solved by the method of successive over relaxation (SOR).

We briefly review here that the nonlinear analysis formulated in [6] essentially computes the third-order coefficient g of the standing wave amplitude equation

 © 2000 The American Physical Society

$$\frac{dA}{dt} = \alpha(f - f_0)A - gA^3. \quad (2)$$

Here A is the wave amplitude, f_0 the threshold, and $\alpha(f - f_0)$ the linear growth rate.

It is most convenient in Faraday waves to use $1/\omega_0$ ($\omega_0 \equiv \omega/2$) as the time scale and $1/k_0$, with k_0 defined by the inviscid dispersion relation $\omega_0^2 = g_r k_0 + \sigma k_0^3/\rho$ [18], as the length scale. The driving amplitude f is measured in units of $4\omega_0^2/k_0$. Since we consider only infinite-depth fluids, the system is characterized by two dimensionless parameters defined as $\Sigma = \sigma k_0^3/\rho\omega_0^2$ and $\gamma = 2\nu k_0^2/\omega_0$. Having the range of $0 \le \Sigma \le 1$, Σ is the measure of the capillarity: $\Sigma = 0$ being the pure gravity wave and $\Sigma = 1$ the pure capillary wave. The second parameter γ is the damping strength.

A typical stability diagram with $\Sigma = 0.6553$ and $\gamma = 0.9505$ is shown in Fig. 1. Marked as $\omega/2$ is the linearly unstable region of the subharmonic excitations with a frequency $\omega_0 = \omega/2$ (similarly for ω and $3\omega/2$). The critical wave number which has the lowest driving threshold is labeled as k_c. This is usually in the subharmonic region, although in certain conditions [5] it is in the harmonic (ω) region. Also labeled as k_a is the tip of the subharmonic region.

We first consider the nonlinearly saturated wave amplitudes. Simulation surface profiles are Fourier transformed to get the saturated amplitude A_m of the primary wave number k, which is set by the lateral dimension of the cell. Weakly nonlinear analysis says that A_m near threshold is expected to scale as the square root of $f - f_0(k)$. In Fig. 2 we show A_m as filled symbols at three wave numbers with $\Sigma = 0.6553$ and $\gamma = 0.095\,05$. At k_c and $0.8k_c$, the agreements are excellent between the limiting slopes near thresholds of the simulation results (filled symbols) and the straight line slopes from the nonlinear analysis [given by α/g in Eq. (2)]. This comparison also gives us confidence on the numerical simulations and amplitude equation computations, both of which are highly nontrivial.

At $1.1k_c$ we see in Fig. 2 that the third-order coefficient g is negative (the negative slope line). The instability from null to wave states becomes a subcritical bifurcation instead of the supercritical ones at smaller wave numbers. The saturated wave amplitudes (solid squares) are consistent with the subcritical picture. There should be a branch of unstable nonlinear states connecting $f_0(1.1k_c) = 0.1426$ at $A_m = 0$ to the solid squares. We can get tight upper and lower bounds of the amplitudes of these unstable nonlinear states by starting simulations at different initial amplitudes, as illustrated in the inset of Fig. 2. These unstable states are plotted in the figure as open squares, and they again agree with the straight line. The hysteresis boundary is then also obtained.

We thus have a bicritical point at a wave number, which we will call k_b, separating supercritical and subcritical bifurcations. What are the implications on experiments? We find that $k_b > k_c$ in all parameter ranges and it is always supercritical at k_c. In a large experimental cell we expect wave excitations at k_c via a supercritical bifurcation under the condition of slowly increasing driving. However, in a finite cell the wave number is restricted to a set of discrete values. The effects of this restriction have already been seen in experiments [11,12,19]. Since k_b is close to k_c, especially at small dampings (cf. Fig. 3), a small shift in k could result in the subcritical region.

Another possibility is that even in a large cell a finite jump of the driving from below the threshold to above can be applied. The excited wave number can then possibly be different from k_c, although there is not much understanding in this aspect yet.

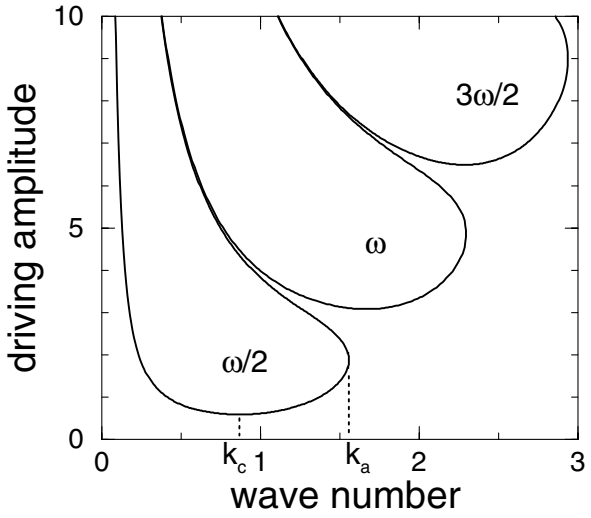

FIG. 1. Neutral stability curves for $\Sigma = 0.6553$ and $\gamma = 0.9505$. Marks $\omega/2$, ω, and $3\omega/2$ represent wave frequencies.

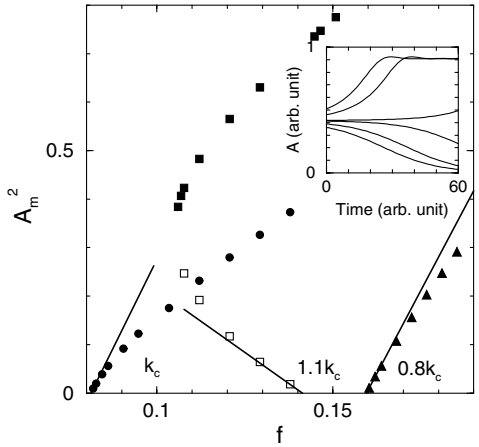

FIG. 2. Nonlinearly saturated wave amplitudes as functions of the driving amplitude at three different wave numbers. The symbols are simulation results and the straight lines are prediction of the nonlinear analysis. Data for $0.8k_c$ are plotted with a shift of $\Delta f = -0.157$. Typical time evolutions of the wave amplitudes at $1.1k_c$ are shown in the inset.

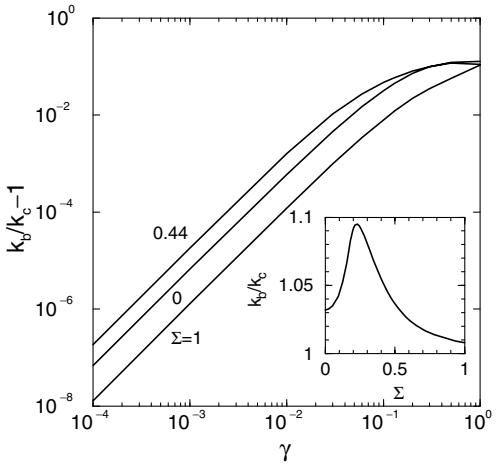

FIG. 3. The bicritical wave number k_b as functions of γ at different Σ. In the inset, $k_b(\Sigma)$ is shown at $\gamma = 0.1$.

The dependence of k_b on Σ is similar for all values of the damping parameter γ. An example is shown in the inset of Fig. 3 with $\gamma = 0.1$. The ratio k_b/k_c is largest for the mixed gravity-capillary wave near $\Sigma = 0.22$ and decreases toward both $\Sigma = 0$ and $\Sigma = 1$.

The dependence of k_b on γ is more interesting. Figure 3 shows three such dependences at $\Sigma = 0$, 0.44, and 1. The difference between k_b and k_c is small, only about 10% even at $\gamma \approx 1$. For example, when water is driven at a frequency of 100 Hz, yielding $\Sigma = 0.89$ and $\gamma = 0.0073$, we have $k_b/k_c - 1 = 8 \times 10^{-5}$.

As $\gamma \to 0$, $k_b \to k_c$. This indicates that the third-order coefficient g in an ideal fluid will be exactly zero at k_0 ($= k_c$ now). Interestingly, this property can be derived from symmetry arguments only: For a *traveling* wave $a_{k_0} \exp(ik_0 x - i\omega_0 t)$ + c.c. in an ideal fluid, symmetries dictate that the evolution equation of a_{k_0} near threshold must be (see, e.g., [8])

$$\dot{a}_{k_0} = -if a^*_{-k_0} + i(T_1|a_{k_0}|^2 + T_2|a_{-k_0}|^2)a_{k_0}. \qquad (3)$$

Here T's are real numbers. Now one can construct the amplitude equation for a *standing* wave, which is what is observed in experiments, from a_{k_0} and a_{-k_0} [(a_{k_0}, a_{-k_0}) having a relative phase of $(1, -i)$]. The resulting third-order coefficient will always be zero. Furthermore, since this property results from symmetries only, we expect similar behaviors for higher frequency excitations (waves excited at $\omega, 3\omega/2, 2\omega, \ldots$). This is indeed confirmed in the numerical simulations of the harmonic responses.

Now we switch our discussion to the waves near k_a. Referring to Fig. 1, when the driving f passes over the upper boundary of the linear instability region, the system becomes linearly stable just as when f is below the threshold value. In principle, numerical simulations can reveal the bifurcation type at this upper branch. Nevertheless, we want to present a generic model as k approaches k_a. At a particular k, when f near the lower and upper thresholds (denoted as f_1 and f_2, respectively) we have two separate amplitude equations,

$$\dot{A} = \delta_i \alpha_i (f - f_i)A - g_i A^3 - h_i A^5, \qquad i = 1, 2, \qquad (4)$$

with $\delta_1 = 1$ and $\delta_2 = -1$. Here $i = 1, 2$ represent the bifurcations at f_1 and f_2, respectively. The fifth-order terms are also included for the possibility of $g_i < 0$.

As $k \to k_a$, f_1 and f_2 approach each other. A single amplitude equation can then be used for k near k_a (with suitable $\beta > 0$),

$$\dot{A} = \beta(f - f_1)(f_2 - f)A - gA^3 - hA^5, \quad k \le k_a \qquad (5)$$

$$= -[(f - f_a)^2 + \delta(k - k_a)]A - gA^3 - hA^5. \qquad (6)$$

In Eq. (6) a generalized linear term also valid for $k > k_a$ (with $\delta > 0$) is modeled, although its detail form is not essential for the validity of the following discussions.

In general, the bifurcations at f_1 and f_2 are not related; as in Eq. (4) they are controlled by the signs of g_1 and g_2 separately. On the other hand, when we have a single equation (5) at $k \to k_a$, they become correlated. Furthermore both nonlinear analysis and numerical simulations as discussed earlier already indicate that g here is negative.

The dynamical picture of the excited waves near k_a following the above equation is illustrated in Fig. 4. At $k < k_a$ (the left diagram) we have subcritical bifurcations at both f_1 and f_2, and the stable nonlinear states are shown as the solid line. Vertical arrows are also drawn to indicate how the amplitude will evolve with time.

At $k = k_a$, the linear term of Eq. (5) becomes zero at $f = f_0$ and is never positive for all f. The dynamics is illustrated in the center diagram of Fig. 4, which may be called the formation of a balloon. When $k > k_a$, the linear term of Eq. (6) is always negative, i.e., the null state is always linearly stable. We get here a detached balloon from the axis as shown in the right diagram. Although the system is now linearly stable for all f, nonlinear states still exist.

Because the picture described in Fig. 4 depends only on a neutral stability curve *turning back* on a particular parameter with subcritical bifurcations, it should happen in any system under similar conditions.

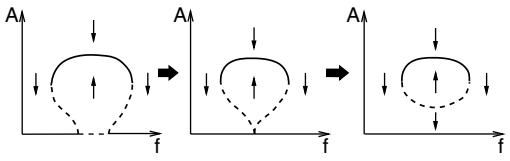

FIG. 4. Formation and detachment of a balloon after the merge of the lower and upper thresholds. The solid lines represent stable nonlinear states, and the dashed lines represent unstable ones. The left diagram corresponds to $k < k_a$, the middle to $k = k_a$, and the right to $k > k_a$.

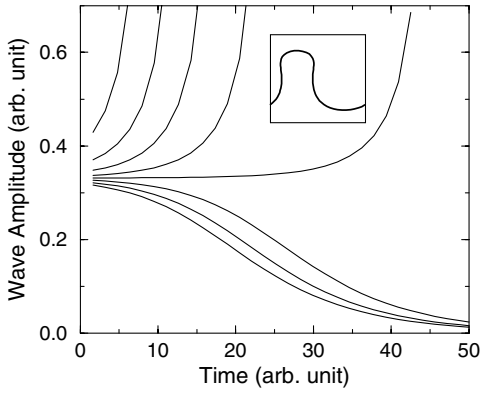

FIG. 5. Time evolutions of wave amplitudes at $k > k_a$. In the inset a typical surface profile of large amplitude states is shown.

We show in Fig. 5 typical simulation results at $k > k_a$. There is the signature of an unstable nonlinear state near $A = 0.33$, corresponding to the lower branch (the dashed line) in the right diagram of Fig. 4. For $A > 0.33$ the amplitude indeed increases and leads to a droplet ejecting state (as shown in the inset of Fig. 5). However, our current simulation code cannot handle the pinch off of a droplet properly.

In conclusion, we first find that at large wave numbers the Faraday wave instabilities become subcritical. Because of the closeness of the critical and bicritical wave numbers, it is expected to be easily observable in experiments. Second, we demonstrate the formation of balloon-shaped nonlinear states when the wave numbers are outside the tip of the instability region. A general argument based on the amplitude equation indicates that this is generic for systems with similar neutral stability curves.

This work is supported by the National Science Council of Taiwan under Contract No. NSC 89-2112-M-008-011.

[1] For a review, see M. C. Cross and P. C. Hohenberg, Rev. Mod. Phys. **65**, 851 (1993).
[2] M. Faraday, Philos. Trans. R. Soc. London **121**, 319 (1831).
[3] T. Benjamin and F. Ursell, Proc. R. Soc. London **225**, 505 (1954).
[4] K. Kumar and L. S. Tuckerman, J. Fluid Mech. **279**, 49 (1994); K. Kumar, Proc. R. Soc. London A **452**, 1113 (1996).
[5] H. W. Müller *et al.,* Phys. Rev. Lett. **78**, 2357 (1997).
[6] P. Chen and J. Viñals, Phys. Rev. Lett. **79**, 2670 (1997); Phys. Rev. E **60**, 559 (1999).
[7] B. Christiansen, P. Alstrøm, and M. T. Levinsen, Phys. Rev. Lett. **68**, 2157 (1992); W. S. Edwards and S. Fauve, Phys. Rev. E **47**, R788 (1993); J. Fluid Mech. **278**, 123 (1994); M. Torres *et al.,* Chaos Solitons Fractals **5**, 2089 (1995); T. Besson, W. S. Edwards, and L. S. Tuckerman, Phys. Rev. E **54**, 507 (1996); A. Kudrolli and J. P. Gollub, Physica (Amsterdam) **97D**, 133 (1996); D. Binks and W. van de Water, Phys. Rev. Lett. **78**, 4043 (1997); D. Binks, M.-T. Westra, and W. van de Water, Phys. Rev. Lett. **79**, 5010 (1997).
[8] S. T. Milner, J. Fluid Mech. **225**, 81 (1991).
[9] J. W. Miles, J. Fluid Mech. **248**, 671 (1993); **269**, 353 (1994); P. L. Hansen and P. Alstrøm, J. Fluid Mech. **351**, 301 (1997).
[10] C. Wagner, H. W. Müller, and K. Knorr, Phys. Rev. Lett. **83**, 308 (1999); H. Arbell and J. Fineberg, Phys. Rev. Lett. **84**, 654 (2000); H.-J. Pi *et al.,* Phys. Rev. Lett. **84**, 5316 (2000).
[11] F. Simonelli and J. P. Gollub, J. Fluid Mech. **199**, 471 (1989); A. D. D. Craik and J. Armitage, Fluid Dyn. Res. **15**, 129 (1995).
[12] S. Douady, F. Fluid Mech. **221**, 383 (1995).
[13] J. W. Miles, J. Fluid Mech. **146**, 285 (1984).
[14] S. P. Decent and A. D. D. Craik, J. Fluid Mech. **293**, 237 (1995).
[15] J. W. Miles, J. Fluid Mech. **75**, 419 (1976).
[16] For further details see, e.g., *Numerical Grid Generation,* edited by J. F. Thompson (North-Holland, Amsterdam, 1982).
[17] See, e.g., C. Pozrikidis, *Introduction to Theoretical and Computational Fluid Dynamics* (Oxford University Press, New York, 1997).
[18] L. D. Landau and E. M. Lifshitz, *Fluid Mechanics* (Pergamon, New York, 1959).
[19] J. Bechhoefer, V. Ego, S. Manneville, and B. Johnson, J. Fluid Mech. **288**, 325 (1995).